Monthly Notices
of the
ROYAL ASTRONOMICAL SOCIETY

MNRAS **428,** 1958–1967 (2013) doi:10.1093/mnras/sts163

Revised SWIRE photometric redshifts

Michael Rowan-Robinson,[1]⋆ Eduardo Gonzalez-Solares,[2] Mattia Vaccari[3,4] and Lucia Marchetti[3]

[1]*Astrophysics Group, Blackett Laboratory, Imperial College of Science, Technology and Medicine, Prince Consort Road, London SW7 2AZ*
[2]*Institute of Astronomy, Madingley Road, Cambridge CB3 0HA*
[3]*Dipartimento di Fisica e Astronomia 'Galileo Galilei', Università di Padova, Vicolo Osservatorio 3, I-35122 Padova, Italy*
[4]*Department of Physics, University of Western Cape, 7535 Belliville, Cape Town, South Africa*

Accepted 2012 October 5. Received 2012 September 17; in original form 2012 July 10

ABSTRACT

We have revised the Spitzer Wide-Area Infrared Extragalactic survey (SWIRE) Photometric Redshift Catalogue to take account of new optical photometry in several of the SWIRE areas, and incorporating Two Micron All Sky Survey (2MASS) and UKIRT Infrared Deep Sky Survey (UKIDSS) near-infrared data. Aperture matching is an important issue for combining near-infrared and optical data, and we have explored a number of methods of doing this. The increased number of photometric bands available for the redshift solution results in improvements both in the rms error and, especially, in the outlier rate.

We have also found that incorporating the dust torus emission into the quasi-stellar object (QSO) templates improves the performance for QSO redshift estimation. Our revised redshift catalogue contains over 1 million extragalactic objects, of which 26 288 are QSOs.

Key words: galaxies: evolution – galaxies: starburst – galaxies: star formation – cosmology: observations – infrared: galaxies.

1 INTRODUCTION

Rowan-Robinson et al. (2008) reported photometric redshifts for over 1 million galaxies in the *Spitzer* SWIRE survey (the SWIRE Photometric Redshift Catalogue, hereafter SPRC) and gave a detailed review of earlier work on photometric redshifts. Subsequently, new results have been reported by Wolf et al. (2008), Brammer et al. (2008), Ilbert et al. (2009) and Salvato et al. (2009), and a comparison of photometric redshift methods has been published by Hildebrandt et al. (2010).

The SWIRE survey consisted of 49 deg^2 of sky surveyed by *Spitzer* at 3.6, 4.5, 5.8, 8.0, 24.0, 70.0 and 160.0 μm. The SWIRE areas in which we had optical photometry and were able to derive photometric redshifts in SPRC were (i) 8.72 deg^2 of European Large Area ISO Survey (ELAIS)-N1 (EN1), in which we had five-band ($U'g'r'i'Z'$) photometry from the Wide Field Survey (WFC), (ii) 4.84 deg^2 of ELAIS-N2 (EN2), in which we had five-band ($U'g'r'i'Z'$) photometry from the WFC, (iii) 7.53 deg^2 of the Lockman Hole, in which we had three-band photometry ($g'r'i'$) from the SWIRE photometry programme, with *U*-band photometry in 1.24 deg^2, (iv) 4.56 deg^2 in *Chandra Deep Field*-South (CDFS), in which we had three-band ($g'r'i'$) photometry from the SWIRE photometry programme, (v) 6.97 deg^2 of the *XMM* Large Scale Structure Survey (*XMM*-LSS), in which we had five-band (*UgriZ*) photometry from Pierre et al. (2007) and (vi) 1.5 deg^2 of ELAIS-S1, in which we have three-band (*B*, *V*, *R*) photometry from Berta et al. (2007). In addition, within *XMM* we had 10-band photometry (*ugrizUBVRI*) from the Vimos-VLT Deep Survey (VVDS) programme of McCracken et al. (2003), Le Févre et al. (2005) (0.79 deg^2) and very deep five-band photometry ($BVRi'z'$) in 1.12 deg^2 of the Subaru/*XMM-Newton* Deep Survey (SXDS; Furusawa et al. 2008). The SWIRE data are described in Surace et al. (2004).[1] The estimated redshifts range from 0 to 6 but the bulk are at $z < 1.5$.

The advent of revised INT WFC *UgriZ* optical fluxes for Lockman, EN1 and EN2 (Gonzalez-Solares et al. 2011), the release of Canada–France–Hawaii Telescope (CFHT) Legacy Survey T0005 MegaCam *ugriz* optical fluxes for *XMM* (http://terapix.iap.fr/cplt/oldSite/Descart/CFHTLS-T0005-Release.pdf) and the UKIDSS Data Release 8 of WFCAM *JK* fluxes for Lockman, EN1 and *XMM*-LSS (Lawrence et al. 2007)[2] make it worthwhile revisiting the SWIRE photometric redshifts in these areas.

The *Spitzer*-selected 'data fusion' catalogues compiled by Vaccari et al. (in preparation) comprise most publicly available photometric and spectroscopic data such as the above in most fields surveyed by *Herschel* as part of the Herschel Multi-tiered Extragalactic Survey (HerMES) (Oliver et al. 2012). TOPCAT[3] was used to merge the SPRC catalogues for Lockman, EN1, EN2 and *XMM*-LSS with the data fusion catalogues, with a 1.5 arcsec search radius, to get the desired photometric data. Not all sources from the original SPRC found matches, mostly because the data fusion selection requires a source to be detected at either 3.6 or 4.5 μm

⋆ E-mail: mrr@imperial.ac.uk

[1] And at http://irsa.ipac.caltech.edu/data/SPITZER/SWIRE/.
[2] http://surveys.roe.ac.uk/wsa/dr8plus-release.html
[3] http://www.star.bris.ac.uk/∼mbt/topcat/

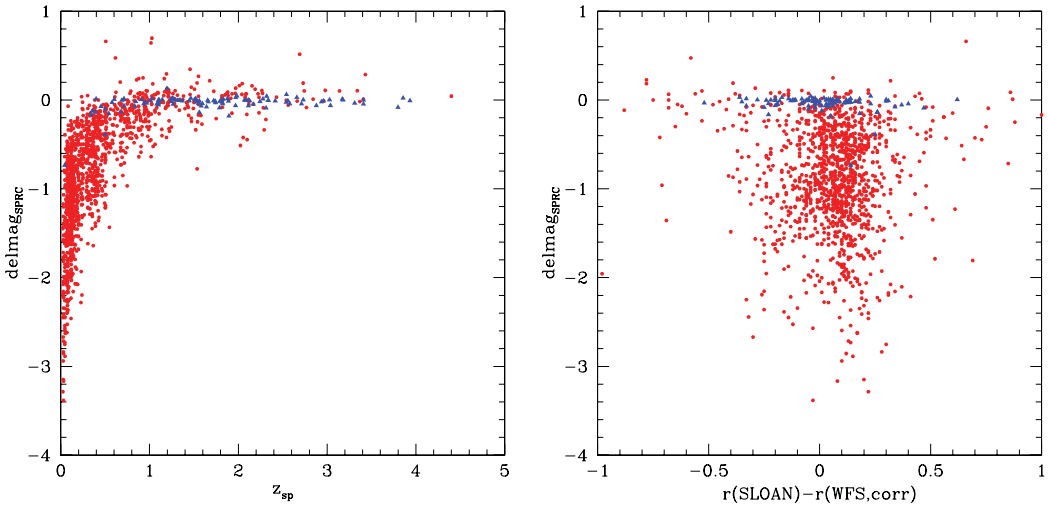

Figure 1. Left-hand panel: SPRC aperture correction versus z_{sp} for Lockman. Right-hand panel: SPRC aperture correction versus r(SDSS, model) − r(WFC, mag-auto). Red symbols: galaxies, blue symbols: QSOs.

and some 24 μm sources from the original SPRC are thus missing from the data fusion catalogues. Table 1 summarizes the optical and near-infrared data available in each SWIRE area.

Rowan-Robinson et al. (2008) used optical magnitudes and *Spitzer*/IRAC 3.6 and 4.5 μm fluxes to estimate photometric redshifts. They reported difficulty in incorporating 2MASS and UKIDSS *J*, *H*, *K* magnitudes into the solution, which they attributed to issues of aperture matching. These problems have been solved here. The use of these additional bands, together with the improved optical photometry, has resulted in a reduction in the number of catastrophic outliers and improved rms values, when photometric and spectroscopic redshifts are compared. Since redshifts are now determined from up to 15 bands, compared with generally a maximum of seven previously, the new redshifts are more reliable. The new catalogues comprise 1 009 607 redshifts, out of a total of 1 066 879 in the original SPRC.

2 APERTURE CORRECTIONS

Aperture matching between wavelength bands is crucial to the success of photometric redshifts. For distant galaxies, photometry in a 2 or 3 arcsec aperture will give the integrated light from the whole galaxy. For nearby galaxies, photometry in the same aperture would be dominated by light from the central regions of the galaxy and might comprise only a few per cent of the integrated light. In template-fitting methods such as the one used here, it is natural to try to seek an estimate of the integrated spectral energy distribution (SED), so that near and distant galaxies can be fitted with the same template. This also has the benefit that derived properties such as luminosity, star formation rate, stellar mass and dust mass have a physical meaning for the galaxy.

Table 1. Explanation of magnitude fields.

Field	am1–5	am21,22,23,25,26	am6–8
EN1	Rev. WFC *UgriZ*	SDSS *ugriz*	2MASS/UKIDSS *JHK*
EN2	Rev. WFC *UgriZ*	SDSS *ugriz*	2MASS *JHK*
Lock	Rev. SWIRE *Ugri*	SDSS *ugriz*	2MASS/UKIDSS *JHK*
VVDS	VVDS *ugri*	*UBVRI*	VVDS *JK*
SXDS	Subaru	MegaCam *ugriz*	–
XMM	SWIRE *UgriZ*	MegaCam *ugriz*	UKIDSS *JHK*
CDFS	SWIRE *gri*	–	–
S1	SWIRE *B*, *V*, *R*	–	–

There are several options for estimating the integrated light from an extended galaxy in any particular waveband. Optical and near-infrared catalogues generally provide Kron and Petrosian integrated magnitudes. SEXTRACTOR (Bertin & Arnouts 1996) provides a mag-auto integrated magnitude (similar to Kron magnitude). These integrated magnitudes are derived essentially by a curve of growth fitted to photometry derived in a series of apertures of different sizes. However, in practice, using integrated magnitude estimates for each photometric band to derive the integrated SED gives poor results for photometric redshifts. This is presumably because of the uncertainty introduced by the process of estimating the integrated magnitude, primarily because of different contributions of sky photon noise. A much more successful option is to start from photometry derived in a single small aperture in each band, and then apply an aperture correction derived in a single chosen band to all the bands. This is the approach followed by Rowan-Robinson et al. (2008) and Gonzalez-Solares et al. (2011).

2.1 Optical data

The optical photometry in SPRC had been derived in most areas using SEXTRACTOR and we used magnitudes measured in a 2 arcsec diameter aperture, applying an *r*-band aperture correction to all bands:

$$\mathrm{delmag_{SPRC}} = r(\text{mag-auto}) - r, \quad (1)$$

where r is measured in a 2 arcsec aperture (WFC 'aper2'). All optical magnitudes used in this work are AB magnitudes and all *J*, *H*, *K* magnitudes are Vega magnitudes (with the exception of the VVDS area, where they are AB magnitudes). The quoted optical and near-infrared magnitudes have been point spread function aperture corrected, to correct for the light lying outside the aperture for a point source (PS). Hereafter, in this paper, we use the term 'aperture correction' to mean the extended source aperture correction. Fig. 1 (left-hand panel) shows the optical aperture correction, $\mathrm{delmag_{SPRC}}$, used in SPRC, versus redshift for the Lockman area, essentially a plot of (inverse) angular size versus redshift. The aperture correction was only applied to the optical magnitudes if it lies in the range −0.10 to −5.0. Otherwise it was set to zero. Sources with

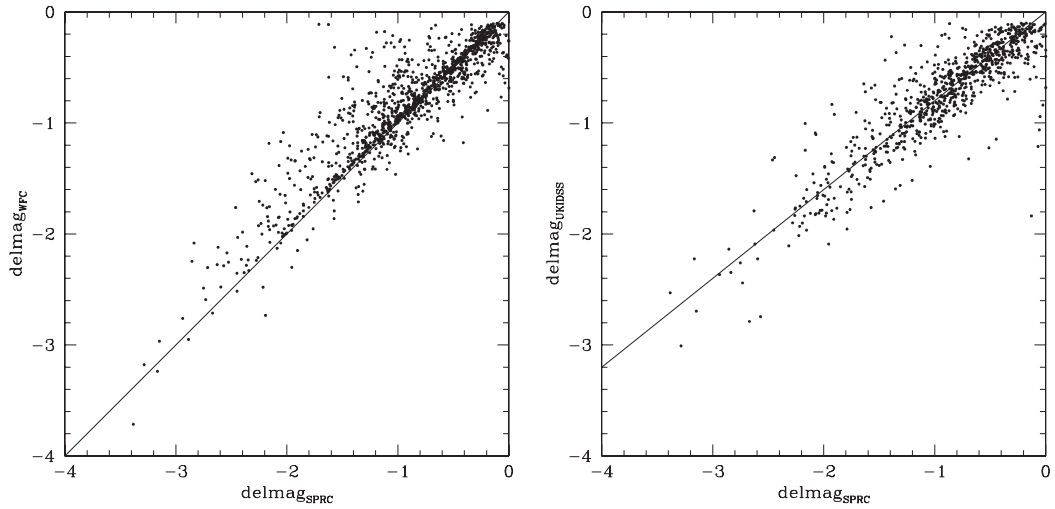

Figure 2. Left-hand panel: plot of delmag$_{WFC}$ (equation 2) versus delmag$_{SPRC}$, the SPRC aperture correction, in Lockman. The straight line has slope 1. Right-hand panel: plot of delmag3 (equation 3) versus delmag$_{SPRC}$, the SPRC aperture correction. The straight line has slope 0.8.

aperture correction >-0.10 mag are considered to be PSs within the uncertainties of the photometric accuracy and the estimation of the integrated magnitude. Sources with aperture correction <-5.0 mag (<0.01 per cent of sources) are considered to be erroneous determinations of integrated magnitude.

For Sloan Digital Sky Survey (SDSS) optical data, available for the Lockman, EN1 and EN2 areas, the 'model' magnitude provides a well-calibrated integrated magnitude. Fig. 1 (right-hand panel) shows delmag$_{SPRC}$ versus r(SDSS, model) $-$ r(WFC, mag-auto). Almost all quasars have no aperture correction, as expected. For galaxies, there is no sign of any correlation of r(SDSS, model) $-$ r(WFC, mag-auto) with delmag$_{SPRC}$, so the SDSS model magnitude is estimating approximately the same total magnitude as the WFC mag-auto. However, there is quite a wide dispersion in r(SDSS, model) $-$ r(WFC, mag-auto), sufficient to harm photometric redshift estimation (see SED plots below, Fig. 14). This dispersion arises from the uncertainties in the two estimates of the integrated magnitude. We have therefore added r(WFC, mag-auto) $-$ r(SDSS, model) to the SDSS model magnitudes to normalize the two sets of aperture corrections. The reason for making the WFC r magnitude the preferred choice is that there are far more SWIRE sources with WFC data than with SDSS data. Also the WFC goes 1 mag deeper than SDSS and therefore provides more accurate magnitudes for fainter SDSS sources. For SDSS data, we investigated using the PS magnitudes, with aperture correction r(SDSS, Petr) $-$ r(SDSS, PS), but this gave inferior results to using the SDSS model magnitudes. This is understandable because the model magnitudes use an aperture derived in the r band and then measure the flux in that aperture in all the bands, ensuring consistent galaxy colours.

We investigated various other options for aperture corrections in the optical. The revised WFC photometry of Gonzalez-Solares et al. (2011), available in the fusion catalogues, includes the Petrosian magnitude in each band, so we define

$$\mathrm{delmag_{WFC}} = r(\mathrm{WFC, Petr}) - r, \quad (2)$$

This is well correlated with delmag$_{SPRC}$ (Fig. 2, left), but with significant scatter.

Using delmag$_{WFC}$ instead of delmag$_{SPRC}$ led to slightly worse phot-z results, so we decided to stick with delmag$_{SPRC}$, which was derived from the SEXTRACTOR r-band mag-auto, for WFC data (while using the revised WFC magnitudes supplied in the fusion catalogue). However, where a mag-auto estimate is not available, we have used delmag$_{WFC}$.

2.2 Near-infrared data

For 2MASS data, an option for the aperture correction is to use the K-iso magnitude if available, and the K-PS magnitude otherwise, with aperture correction

$$\mathrm{delmag_{2MASS}} = K(\mathrm{2MASS, iso}) - K(\mathrm{2MASS, PS}). \quad (3)$$

For UKIDSS data, the natural aperture correction to consider is

$$\mathrm{delmag_{UKIDSS}} = K(\mathrm{UKIDSS, Petr}) - K(\mathrm{UKIDSS, aper3}), \quad (4)$$

applied to the aper3 (1.0 arcsec) J, K magnitudes.

Both delmag$_{2MASS}$ and delmag$_{UKIDSS}$ are quite well correlated with delmag$_{SPRC}$ (Fig. 2, right-hand panel, shows the correlation of delmag$_{UKIDSS}$ with delmag$_{SPRC}$) and this suggests the idea of using $k \times$ delmag$_{SPRC}$ as the near-infrared aperture correction, with k to be determined for each survey. The direct use of delmag$_{2MASS}$ and delmag$_{UKIDSS}$ for 2MASS and UKIDSS magnitudes, respectively, resulted in a worse phot-z solution, so the use of $k \times$ delmag$_{SPRC}$ was explored in some detail.

Fig. 3 shows delmag$_{SPRC}$ versus $(z - J)$, with no aperture correction applied to J. There is a very strong correlation. Fig. 4 (left-hand panel) shows delmag$_{SPRC}$ versus $(z - J)$ for 2MASS data, with an aperture correction $0.8 \times$ delmag$_{SPRC}$ applied to J. Fig. 4 (right-hand panel) shows delmag$_{SPRC}$ versus $(z - J)$ for UKIDSS data, with an aperture correction $1.1 \times$delmag$_{SPRC}$ applied to J. Only sources with spectroscopic redshift <0.3 have been included to minimize the possibility of evolution of colour with angular size. We can see that these corrections work well in removing the correlation of colour with delmag$_{SPRC}$.

2.3 IRAC data

In SPRC, we used Kron fluxes if the 3.6 μm size was greater than a specified threshold (area $>$ 200 pixels), otherwise we used 'IRAC aper2' fluxes (measured in a 3.8 arcsec aperture). For sources smaller than this threshold, the Kron and aper2 magnitudes agreed well. This is also the approach adopted here. Fig. 5 shows delmag$_{SPRC}$ versus [K-am(3.6 μm)] for 2MASS (left-hand panel) and UKIDSS (right-hand) data, where am(3.6μm) is the AB

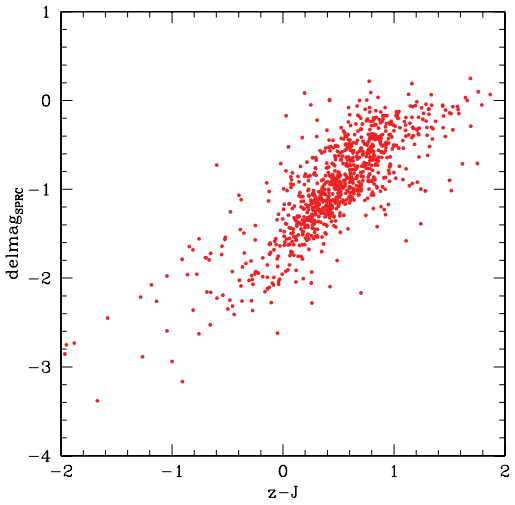

Figure 3. SPRC aperture correction versus $z - J$, with no aperture correction applied to J.

magnitude derived from the *Spitzer* 3.6μm flux. There are some residual issues for the UKIDSS–IRAC comparison. This does harm the photometric redshift estimates for some objects, resulting in a larger reduced χ^2 for the fit. SED fits for selected galaxies with $\chi^2 > 5$ with known spectroscopic redshift show that the IRAC fluxes give good consistency with the aperture-corrected optical magnitudes. The problem lies with overestimation of the J, H and especially K brightness for extended galaxies. Changing the IRAC aperture correction to $k \times \mathrm{delmag_{SPRC}}$ improved the appearance of Fig. 6 (right-hand panel) enormously, but led to worse phot-z results. The main problem was an offset of the $\log_{10}(1 + z_{\mathrm{phot}})$ points relative to $\log_{10}(1 + z_{\mathrm{spect}})$ by ∼0.01. This was not fixed by the process of in-band correction factors (Ilbert et al. 2006), and it would probably be necessary to revise the templates in the near-infrared to achieve convergence.

3 PHOTOMETRIC REDSHIFTS

The photometric redshift method is as described in SPRC. It is a two-pass template method based on six galaxy (11 in the second pass) and three AGN templates. The galaxy templates were first generated empirically, then modelled with a full star formation history so that star formation rates and stellar masses can be derived. After the first pass, the infrared excess relative to the starlight fit is modelled with four infrared SED types (Cirrus, M82 starburst, Arp 220 starburst and AGN dust torus). Dust extinction with A_V ranging up to 1.0 is permitted. For quasi-stellar object (QSOs), Small Magellanic Cloud (SMC) dust properties are assumed.

For galaxies and QSOs, *JHK* magnitudes and 3.6 and 4.5 μm fluxes were used in the first pass through the data provided there was no evidence of a strong AGN dust torus component, which was determined by the condition $S(5.8) > 1.2\,S(3.6)$. For galaxies, these near-infrared data were not used in the second pass fit if the dust torus component was dominant at 8 μm from the infrared template fitting. For the second pass for QSOs, a new approach was developed, described in Section 4 below, to allow use of the near-infrared data even though a dust torus component is present.

In the photometric redshift solution, we used the new SDSS 'model' magnitudes, and the revised WFC magnitudes, but we retained the WFC star/galaxy classification in each band (because this information is available for a much higher proportion of sources) and the optical aperture correction used in SPRC. We used 2MASS *JHK* (Point Source Catalog), if available, and UKIDSS *JK* (aper3) if not.

We used galaxies with known spectroscopic redshifts to determine in-band correction factors, following Ilbert et al. (2006). These are shown in Table 2. Spectroscopic redshifts came from a wide range of references (details are given in the online catalogue) and are mostly in the range 0–1.2 for galaxies.

Fig. 6 shows a comparison of the SDSS $\log_{10}(1 + z_{\mathrm{phot}})$ with $\log_{10}(1 + z_{\mathrm{spect}})$ for the SWIRE Lockman sample (left-hand panel) and the same plot for the present sample (right-hand panel). The SDSS performance is better at $z < 0.3$, but our approach works better at $z > 0.5$. To improve our photometric redshifts at $z < 0.3$, it would be necessary to refine our optical templates using the new photometric data and to increase the number of templates. The latter would be likely to worsen the performance at higher redshift through increased aliasing.

Fig. 7 (left-hand panel) shows the same comparison for the SPRC, restricted to $r < 23.5$, reduced $\chi^2 < 3$ and at least five photometric bands in the solution. Fig. 7 (right-hand panel) shows a similar

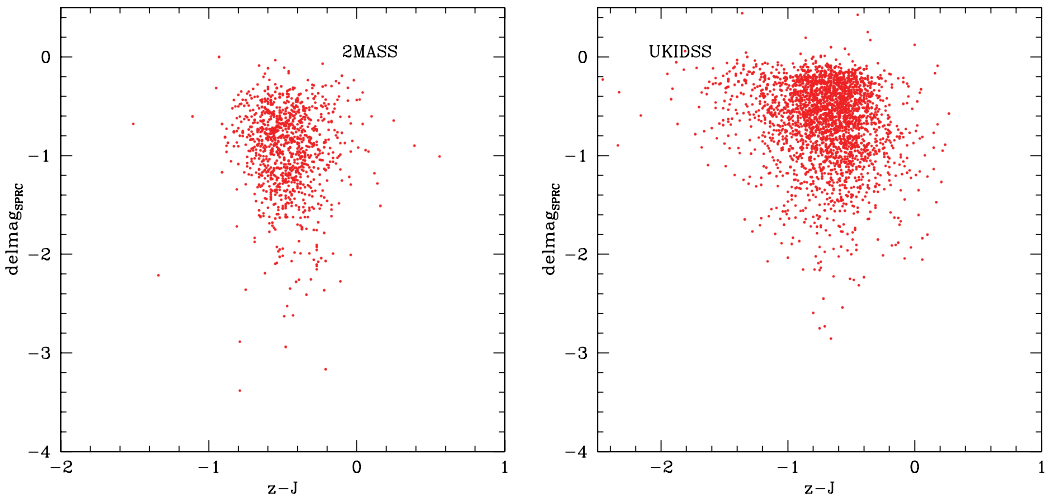

Figure 4. Left-hand panel: SPRC aperture correction versus corrected ($k = 0.8$) $z - J$ for 2MASS. Right-hand panel: SPRC aperture correction versus corrected ($k = 1.1$) $z - J$ for UKIDSS. Only sources with spectroscopic redshift <0.3 have been included to minimize the possibility of evolution of colour with angular size.

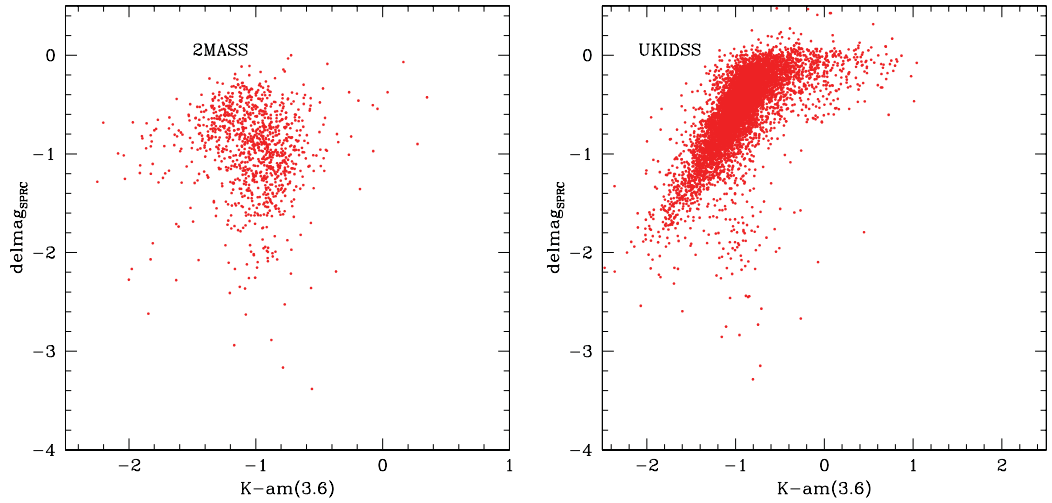

Figure 5. Left-hand panel: SPRC aperture correction versus corrected ($k = 0.7$) K-am(3.6) for 2MASS. Right-hand panel: SPRC aperture correction versus corrected ($k = 1.1$) K-am(3.6) for UKIDSS. Only sources with spectroscopic redshift <0.3 have been included to minimize the possibility of evolution of colour with angular size.

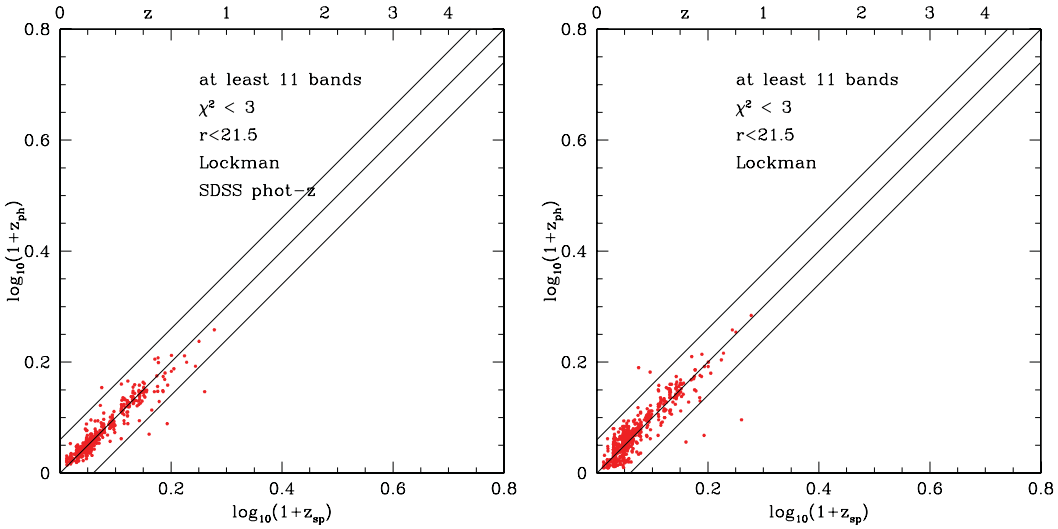

Figure 6. Left-hand panel: SDSS photometric redshifts versus spectroscopic redshifts for Lockman SWIRE sample. Right-hand panel: photometric redshifts from present work versus spectroscopic redshifts for Lockman SWIRE sample.

Table 2. Correction factors for fluxes in each band, by area.

Area	U'	g'	r'	i'	Z'	J	H	K	3.6 μm	4.5 μm
EN1,EN2	1.354	1.135	1.104	1.059	0.650	0.976	0.900	0.888	1.071	1.104
Lockman	1.360	1.062	0.982	0.922		0.923	0.904	0.899	1.036	1.066
VVDS	1.046	0.969	0.928	0.960	0.972	1.173		1.029	1.085	1.015
XMM-LSS	1.308	1.206	1.056	0.925	1.011				1.085	1.086
CDFS	1.046	0.969	0.916	0.991	0.972				1.238	1.037

plot for the revised SPRC, with the requirement that K be selected, and for a minimum of seven photometric bands. We can see that inclusion of near-infrared (*JHK*) data in the solution has reduced the number of catastrophic outliers.

Fig. 8 (left-hand panel) shows the same comparison for the revised catalogue in *XMM*, with at least nine bands in the solution. Fig. 8 (right-hand panel) shows the same comparison for photometric redshifts from the LePhare method (Ilbert et al. 2006). The latter results are better for $z < 0.5$, but worse for $z > 0.5$. Again, this is probably the consequence of the larger number of templates used by Ilbert et al.

4 QSOS

The SPRC approach required that an object be flagged as stellar to consider a QSO optical template. With the SPRC stellar flag, some QSOs get missed (and end up with the wrong redshift) as a result of this condition. As discussed in SPRC, it is not possible to

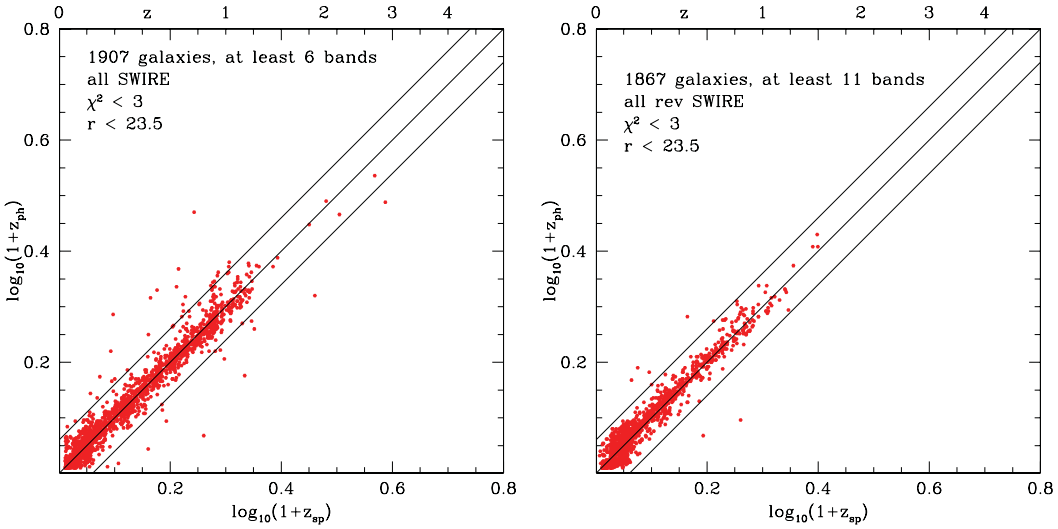

Figure 7. Left-hand panel: photometric redshifts from SPRC (Rowan-Robinson et al. 2008) for galaxies with $r < 23.5$, at least six photometric bands, reduced $\chi^2 < 3$. Red symbols: galaxies. Right-hand panel: same for revised SPRC, with at least 11 photometric bands.

allow a QSO template option for all galaxies, since far too many galaxies end up with mistakenly high redshifts. However, while still requiring a stellar flag for an object to select a QSO template, we have allowed the SDSS stellar flag to override the WFC flag where they disagree and this allows a few more quasars through.

Salvato et al. (2009) have demonstrated excellent performance for 1032 QSOs and AGN in the COSMOS field, using 30 photometric bands, including 12 narrow-band filters. They introduce two innovations: first, they track the variability of quasars and apply an appropriate correction to the photometry. Secondly, they use templates that include a range of contributions from AGN dust tori.

While we do not have the information to track QSO variability in our photometry, we have explored the idea of adding a range of AGN dust tori strengths to our QSO templates during the second pass, and then using the 1.25–8 μm data in the redshift solution. The amplitude of dust tori added corresponded to $L_{\rm tor}/L_{\rm opt} = 0, 0.2, 0.4, 0.6, 0.8$ and 1.0. The performance for QSOs is much improved (Fig. 9), especially in the reduction of catastrophic outliers. For at least 11 photometric bands, reduced $\chi^2 < 3$, $r < 21.5$, we find an rms of 9.3 per cent and an outlier rate of 9.3 per cent. For comparison, Salvato et al. (2009), with 30 bands, achieved an rms of 1.2 per cent for QSOs with $I < 22.5$ and an outlier rate of 6.3 per cent. Their greatly improved rms can be attributed to the correction for variability and to the use of 30 photometric bands, including 12 narrow-band filters. However, our outlier performance is almost as good, despite less than half the number of photometric bands.

5 REASONS FOR POOR χ^2

Although the photometric redshift estimates are good for sources where the reduced $\chi^2 < 3$, the estimates get slightly worse as χ^2 increases and some sources have very large χ^2. We have investigated the reasons for poor χ^2 through colour–colour diagrams and SED plots. The main reasons found for poor χ^2 are (i) contamination by stars, (ii) poor photometry, (iii) QSOs misclassified as galaxies

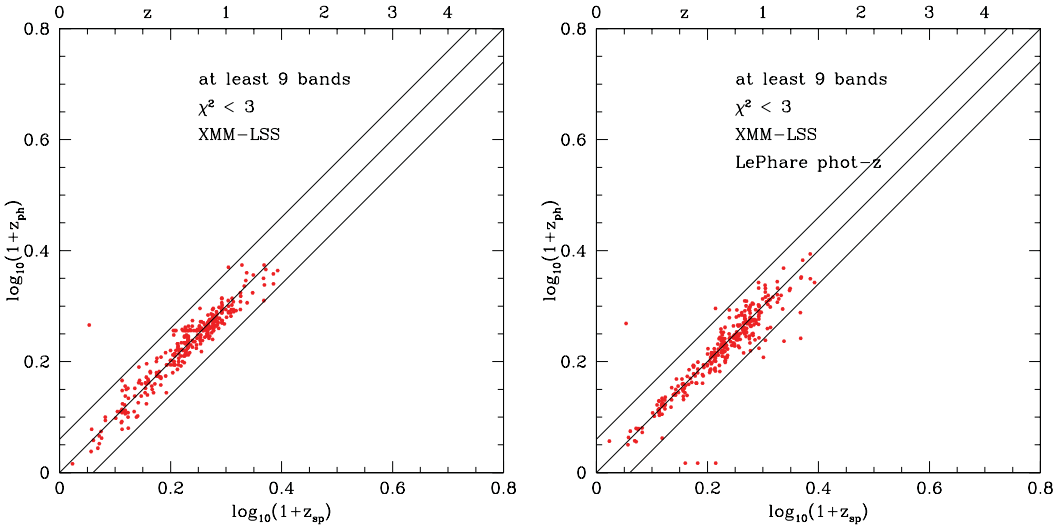

Figure 8. Left: photometric redshifts in *XMM*-LSS using new fusion catalogue: *ugriz* from SDSS, revised *ugri* from WFC, *JHK* from 2MASS, *JK* from UKIDSS. Right: photometric redshifts from LePhare method (Ilbert et al. 2009).

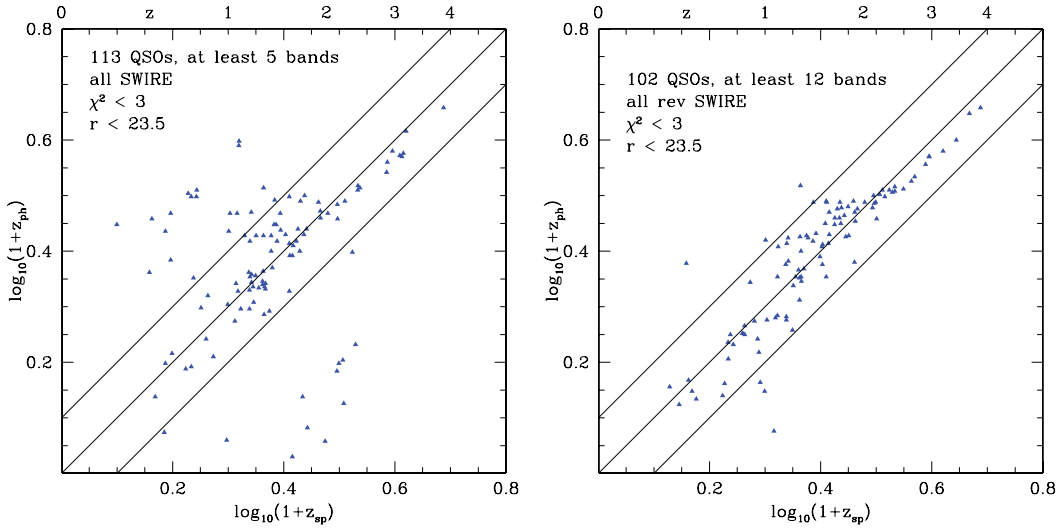

Figure 9. Left-hand panel: photometric redshifts from SPRC (Rowan-Robinson et al. 2008) for quasars with $r < 23.5$, at least seven photometric bands, reduced $\chi^2 < 3$. Blue symbols: QSOs. Right-hand panel: same for revised SPRC, with at least 12 photometric bands.

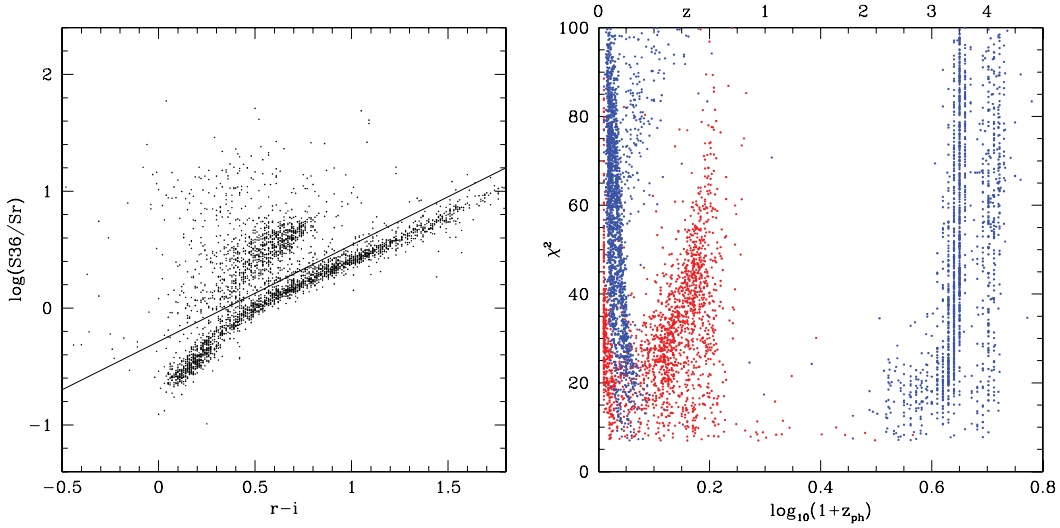

Figure 10. Left-hand panel: ratio of 3.6 μm to r-band flux versus $r - i$ for whole catalogue, for sources with $\chi^2 > 20$ and at least 12 photometric bands. A clear stellar sequence is seen. Stars have been excluded from the catalogue by removing objects flagged as point sources lying below the solid line. Right-hand panel: reduced χ^2 versus estimated photometric redshift for sources classified as stars. Red symbols: sources which the photometric redshift code identified as galaxies; blue symbols: QSOs.

and (iv) QSOs for which the extinction is higher than the maximum assumed $A_V = 1$.

Stars can be recognized in a plot of the ratio of 3.6 μm to r-band flux versus $r - i$ (Fig. 10, left; see Rowan-Robinson et al. 2005). A clear stellar sequence can be seen. We have removed stars from the catalogue by excluding 17 326 sources with stellar flags which lie below the solid line in Fig. 10 (left-hand panel) and which had reduced $\chi^2 > 7$. Fig. 10 (right-hand panel) shows the χ^2 and photometric redshift generated for these candidate stars by the photometric code. Stars can generate spectacularly bad χ^2 and tend to alias with specific galaxy and QSO redshifts. We believe that few of the sources with $\chi^2 < 7$ are stars.

Fig. 11 (left) shows $(u - g)$ versus $(g - r)$ (WFC photometry) for QSOs, with blue symbols for sources with $\chi^2 < 3$ and red symbols for $\chi^2 > 7$, after removal of stars using the 3.6 μm $(r - i)$ constraint. The broken locus is for blackbodies with temperature ranging from 3000 to 15 000 K, the solid locus shows the effect of extinction using SMC dust properties. The $\chi^2 > 7$ objects show a much wider range of colours than those with $\chi^2 < 3$. Examination of SED plots shows that most of the $\chi^2 > 7$ objects are stars with slightly higher 3.6 μm fluxes than the stellar sequence in Fig. 10 (left). A few are QSOs with higher extinction than the maximum $A_V = 1$ we have used. Others have high χ^2 simply because of poor photometry or SED shapes differing from our templates.

Fig. 11 (right) shows $(u - g)$ versus $(g - r)$, for galaxies with SDSS photometry, with different symbols for $\chi^2 < 3$ and $\chi^2 > 7$. About 10 per cent of 'galaxies' with $\chi^2 > 7$ achieved much improved fits with QSO templates (some of these did not have the stellar flag that was a prerequisite for consideration as a QSO). Some are stars with slightly higher 3.6 μm fluxes than the stellar sequence in Fig. 10 (left). For the rest the problem

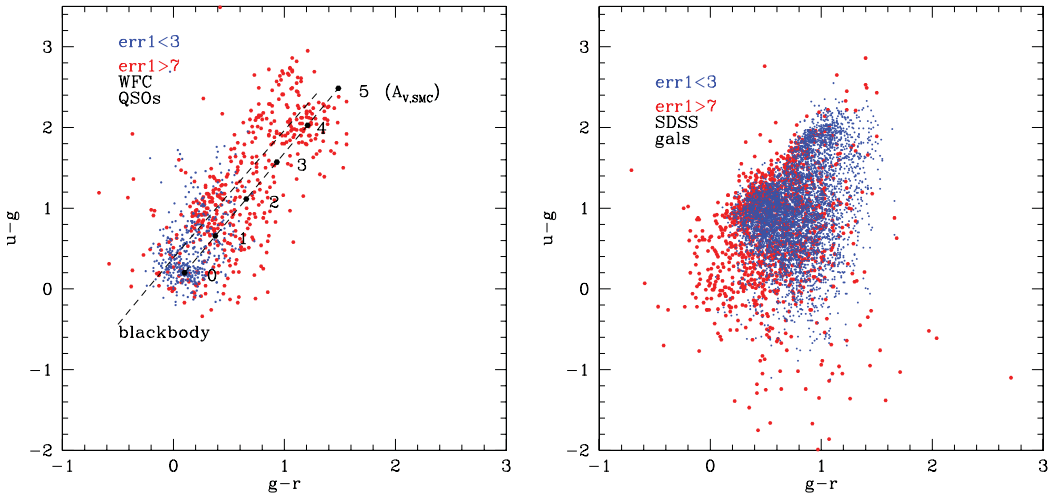

Figure 11. Left-hand panel: $(u - g)$ versus $(g - r)$ (WFC photometry) for QSOs in EN1 field with at least 11 photometric bands, with blue symbols for sources with $\chi^2 < 3$ and red symbols for $\chi^2 > 7$, after removal of stars using the 3.6 μm $(r - i)$ constraint. The broken locus is for blackbodies with temperature ranging from 3000 to 15 000 K, the solid locus shows the effect of extinction (A_V=0–5) assuming SMC dust properties. Right-hand panel: reduced χ^2 versus estimated photometric redshift for sources classified as stars. Red symbols: sources which the photometric redshift code identified as galaxies; blue symbols: QSOs.

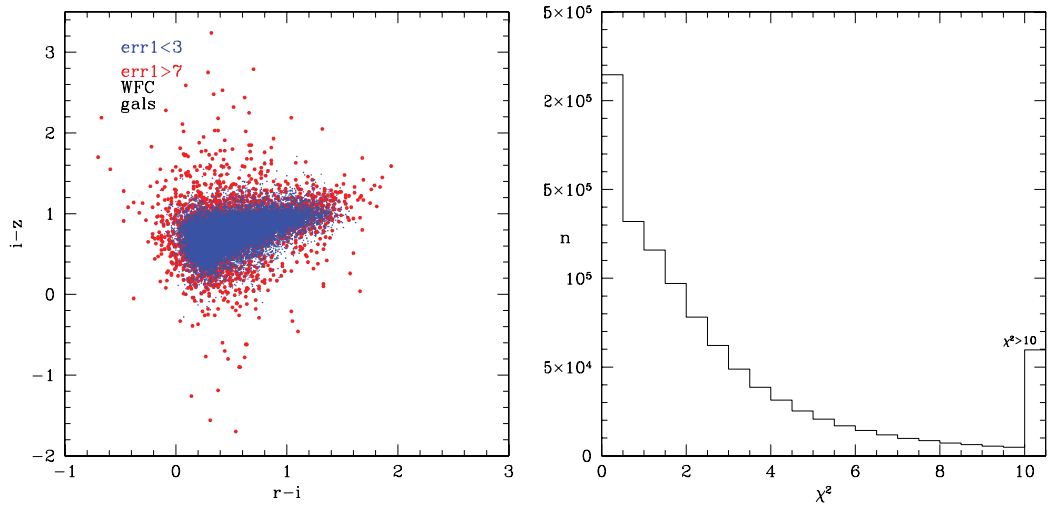

Figure 12. Left: $(i - z)$ versus $(r - i)$, WFC photometry, for galaxies with at least 11 photometric bands and $\chi^2 > 7$ (red) and $\chi^2 < 3$ (blue). Right: histogram of reduced χ^2 for EN1 area, after exclusion of stars.

appears to be poor photometry (and underestimated photometric errors).

Fig. 12 (left) shows $(i - z)$ versus $(r - i)$ (WFC photometry) for galaxies in EN1 with at least 11 photometric bands, with different symbols for $\chi^2 < 3$ and $\chi^2 > 7$. The galaxies with higher χ^2 show a wider spread in colours, suggesting the main issue is photometric problems. Fig. 12 (right-hand panel) shows a histogram of the reduced χ^2 for sources in the EN1 area, after removal of stars.

6 REVISED SWIRE PHOTOMETRIC REDSHIFT CATALOGUE

Our revised SPRC contains 818 555 objects, 204 421 in EN1, 116 195 in EN2, 217 461 in Lockman and 280 478 in *XMM*-LSS, compared with 875 353 in the same areas in the original SPRC. 3.6 per cent of SPRC sources did not find a match in the fusion catalogues, mainly because the latter omitted 24 μm only sources. A further 1 per cent failed to achieve a redshift solution, either because there were less than two valid photometric bands or because the reduced $\chi^2 > 100$. The SWIRE redshifts in CDFS and S1 have not been revised because we have no new photometric information in these areas. These two areas bring the total number of redshifts in the revised catalogue[4] to 1 009 607, with readmeSWIRErev in same directory. Our new catalogue delivers photometric redshifts for 26 288 quasars.

Fig. 13 (left-hand panel) shows a histogram of the number of photometric bands for the new catalogue, compared with that for the SPRC. Fig. 13 (right) shows the redshift distribution of galaxies and quasars in the new catalogue. Although most of the galaxy redshifts are at $z < 1.5$, there is a broad tail to higher redshift. Our

[4] http://astro.ic.ac.uk/∼mrr/swirephotzcat/zcatrev12ff2.dat.gz

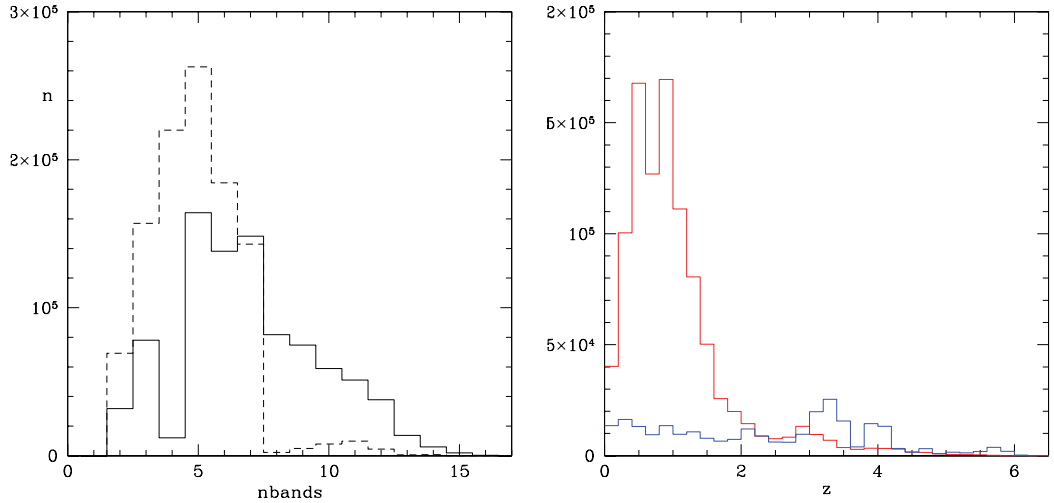

Figure 13. Left-hand: histogram of number of bands used in estimating photometric redshifts in revised catalogue (solid line) compared with SPRC (broken line). Right: histogram of redshifts in revised SPRC (red: galaxies, blue: QSOs, x 10).

Table 3. $z_{\rm phot}$ versus $z_{\rm spect}$ outliers whose SEDs are plotted in Fig. 10, from bottom.

RA	Dec.	$z_{\rm spec}$	Ref.	$z_{\rm phot}$	No. of bands	Notes
161.30797	58.74822	0.2470	1	0.52	12	Alias
161.72533	58.99032	0.1890	1	0.55	12	Alias
161.74496	58.94529	0.8220	1	0.25	12	$z_{\rm spec}$ error?
161.94997	59.29018	0.5600	2	0.17	13	$z_{\rm spec}$ error?
36.40352	−4.39069	0.1307	3	0.85	9	$z_{\rm spec}$ error (single line)?
36.47719	−4.36419	0.8277	3	1.24	9	$z_{\rm spec}$ error (single line)?
248.47900	41.48283	0.1592	4	0.47	14	Need Sab with $A_V = 0.35$

References. (1) Owen & Morrison (2009). (2) Rowan-Robinson et al. (2008). (3) Le Févre et al. (2005). (4) Rowan-Robinson et al. (2004).

catalogue is a very significant resource for galaxies at high redshift, with 106 537 sources with $z > 2$ and 15 226 sources with $z > 4$.

7 SEDS OF OUTLIERS

To investigate outliers, we have plotted in Fig. 14 the SEDs of eight outliers from the $z_{\rm phot}$ versus $z_{\rm spec}$ comparisons, those with $\chi^2 < 3$ and with more than 12 photometric bands in EN1, EN2 and Lockman, and with more than nine bands in *XMM*-LSS. SDSS photometry (after applying the aperture correction of Section 2.1) is shown in red. Details of the sources are given in Table 3. Two objects have aliases at the spectroscopic redshift, one appears to need an Sab template with A_V =0.35 (A_V is set to zero for the Sab template in our code), and four could be errors in the spectroscopic redshift (two were based on a single line).

8 DISCUSSION

With the changes discussed in the previous sections, we now see improvements in the fraction of catastrophic outliers in the photometric redshift estimates. The rms errors for galaxies are very similar to those achieved in SPRC, while those for quasars are significantly improved.

For galaxies with reduced $\chi^2 < 3$, $r < 23.5$, the rms in $(z_{\rm phot} - z_{\rm spec})/(1 + z_{\rm spec})$, after rejection of outliers with values discrepant by 15 per cent or more, are 3.7 and 3.4 per cent, for number of bands 10 and 14, respectively. The corresponding percentages of outliers are 1.2 and 0.2 per cent, respectively. Fig. 15 (left-hand panel) shows how the percentage of outliers for galaxies with $|\log_{10}(1 +$

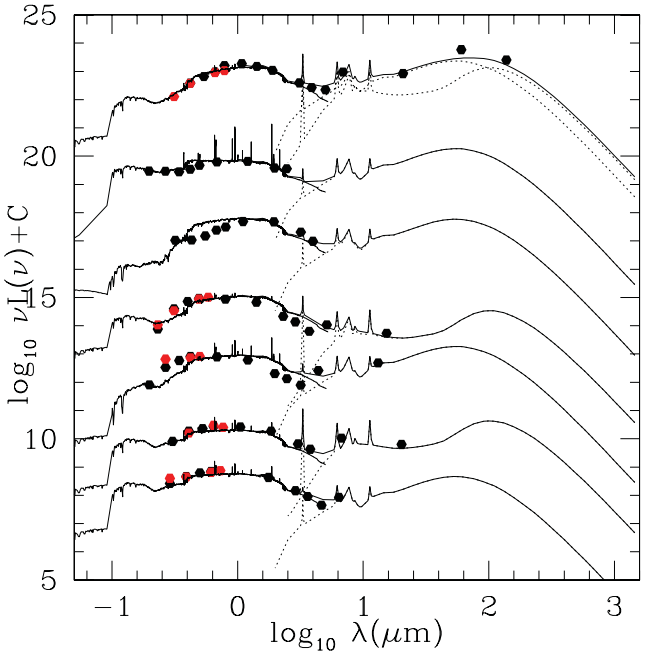

Figure 14. SEDs of outliers in $z_{\rm phot}$ versus $z_{\rm spect}$ plot, using the spectroscopic redshift, with details of sources given in Table 1. Outliers with more than 12 photometric bands in EN1, EN2 and Lockman, and more than nine bands in *XMM*-LSS are included.

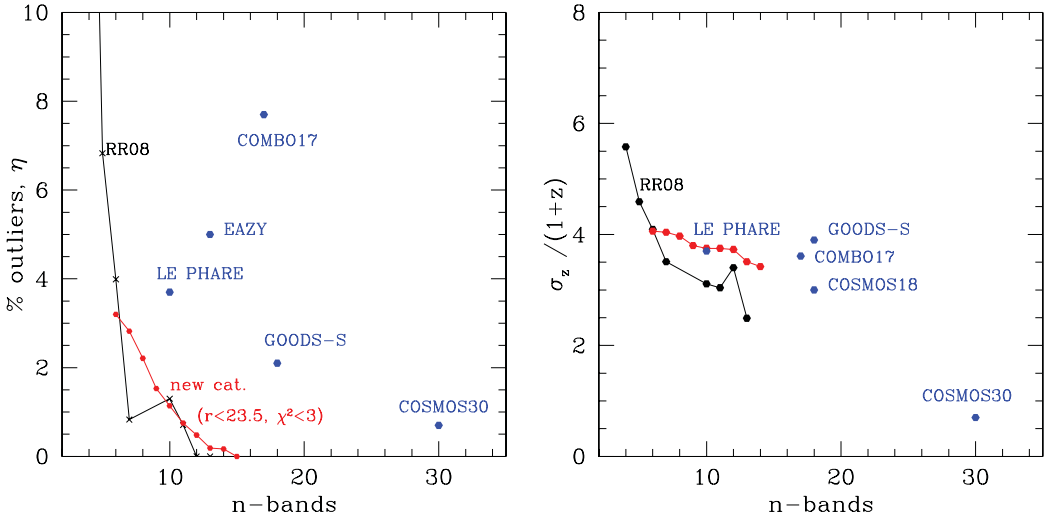

Figure 15. Left: percentage of outliers versus number of photometric bands for SPRC (black loci) and for fusion catalogue (red loci), for sources with reduced $\chi^2 < 3$, $r < 23.5$. Right: percentage rms $[\sigma_z/(1+z)]$ for SPRC (black loci) and for fusion catalogue (red loci), for sources with reduced $\chi^2 < 3$, $r < 23.5$.

$z_{\rm phot})/(1+z_{\rm spect})| > 0.06$ varies with the number of photometric bands. Fig. 15 (right-hand panel) shows the percentage rms $[\sigma_z/(1+z)]$ versus number of photometric bands. The additional photometric bands provided by the *JHK* data from 2MASS and UKIDSS now have a clear beneficial effect, especially on the fraction of catastrophic outliers. Our results can be compared directly with the corresponding results for SPRC, and with new results from EAZY (Brammer et al. 2008), GOODS-S (Dahlen et al. 2010), and COSMOS30 (Ilbert et al. 2009). While these comparisons can be affected by differences in the survey depths, the main differences between these surveys is the number of photometric bands. Our outlier performance is consistently better than other methods.

Our new SWIRE redshift catalogue should be useful for improved studies of the infrared extragalactic population and for the *Herschel* surveys carried out in all of the SWIRE fields by the HerMES consortium.

ACKNOWLEDGMENTS

We thank the SWIRE team for their achievement in delivering the SWIRE Catalogue. We thank the referee for helpful comments that led to improvements in the paper.

REFERENCES

Berta S. et al., 2007, A&A, 467, 565
Bertin E., Arnouts S., 1996, A&A, 117, 393
Brammer G. M. et al., 2008, ApJ, 686, 503
Dahlen T. et al., 2010, ApJ, 724, 425
Furusawa H. et al., 2008, ApJS, 176, 1
Gonzalez-Solares E. et al., 2011, MNRAS, 416, 927
Hildebrandt H. et al. 2010, A&A, 523, 31
Ilbert O. et al., 2006, A&A, 457, 8411
Ilbert O. et al., 2009, ApJ, 609, 1236
Lawrence A. et al., 2007, MNRAS, 379, 1599
Le Févre O. et al., 2005, A&AS, 207, 6334
McCracken H. J. et al., 2003, A&A, 410, 17
Oliver S. J. et al., 2012, MNRAS, 424, 1614
Owen F. N., Morrison G. E., 2009, ApJS, 182, 625
Pierre M. et al., 2007, MNRAS, 382, 279
Rowan-Robinson M. et al., 2004, MNRAS, 351, 1290
Rowan-Robinson M. et al., 2005, AJ, 129, 1183
Rowan-Robinson M. et al., 2008, MNRAS, 386, 687
Salvato M. et al., 2009, ApJ, 690, 1250
Surace J. et al., 2004, The SWIRE N1 Image Atlases and Source Catalogs. Spitzer Science Center, Pasadena
Wolf C., Hildebrandt H., Taylor E. N., Meisenheimer K., 2008, A&A, 492, 933

This paper has been typeset from a TEX/LATEX file prepared by the author.